Constructing Hierarchical Interfaces: TiO$_2$-Supported PtFe–FeO$_x$ Nanowires for Room Temperature CO Oxidation

Huiyuan Zhu,*,[†] Zili Wu,[†,‡] Dong Su,[⊥] Gabriel M. Veith,[§] Hanfeng Lu,[#] Pengfei Zhang,[†] Song-Hai Chai,[∥] and Sheng Dai*,[†,∥]

[†]Chemical Sciences Division, [‡]Center for Nanophase Materials Sciences, and [§]Materials Science and Technology Division, Oak Ridge National Laboratory, Oak Ridge, Tennessee 37831, United States

[∥]Department of Chemistry, University of Tennessee, Knoxville, Tennessee 37996, United States

[⊥]Center for Functional Nanomaterials, Brookhaven National Laboratory, Upton, New York 11973, United States

[#]Institute of Catalytic Reaction Engineering, College of Chemical Engineering, Zhejiang University of Technology, Hangzhou, Zhejiang 310014, China

S *Supporting Information*

ABSTRACT: In this communication, we report a facile approach to constructing catalytic active hierarchical interfaces in one-dimensional (1D) nanostructure, exemplified by the synthesis of TiO$_2$-supported PtFe–FeO$_x$ nanowires (NWs). The hierarchical interface, constituting atomic level interactions between PtFe and FeO$_x$ within each NW and the interactions between NWs and support (TiO$_2$), enables CO oxidation with 100% conversion at room temperature. We identify the role of the two interfaces by probing the CO oxidation reaction with isotopic labeling experiments. Both the oxygen atoms (Os) in FeO$_x$ and TiO$_2$ participate in the initial CO oxidation, facilitating the reaction through a redox pathway. Moreover, the intact 1D structure leads to the high stability of the catalyst. After 30 h in the reaction stream, the PtFe–FeO$_x$/TiO$_2$ catalyst exhibits no activity decay. Our results provide a general approach and new insights into the construction of hierarchical interfaces for advanced catalysis.

The interfacial synergy, typically between metal nanoparticles (NPs) and the supporting metal oxide, determines the active site in heterogeneous catalysis. The critical role of the interface between the oxide and metal has been spotlighted by many previous studies. For example, TiO$_2$ and CeO$_2$ are reported to be active supports for Au and Pt in CO oxidation by activating oxygen or supplying oxygen atoms at the metal NP–support interface.[1−5] The conventional approach to fabricating such an interface is either in situ growth or direct assembly of metal NPs onto oxide supports, which provides limited interfacial effects. Many efforts have been put to design and construct the interfaces at the atomic level to maximize the interfacial synergy and the catalytic performance. A typical strategy is to use small NPs that provide high surface area on each NP and abundant interfaces between NPs and support.[6−9] However, once the NPs' size decreases, the surface energy dramatically increases. This often makes the NPs highly active and, at the same time, unstable (NPs tend to sinter or aggregate) when exposed to chemical and thermal treatment.[10] A more intriguing approach is to tailor the atomic level interface directly on the surface of NPs. For instance, Pt-FeNi(OH)$_x$ interface can be created by integrating a submonolayer of FeNi(OH)$_x$ onto small Pt NPs.[11] Even though these strategies have advanced the fabrication of metal–support interface, one paramount question remains unanswered, that is, whether there is a catalyst motif that could simultaneously provide the high active surface area (small NPs) and good stability under thermal or chemical treatment (large NPs) with abundant atomic level interfaces.

The ultrathin one-dimensional (1D) nanowires (NWs) with the diameter less than 5 nm and the length larger than 20 nm have emerged as a new class of nanocatalysts with impressive activity and durability, demonstrated by their superior performance in fuel cell reactions.[12,13] The structural anisotropy of 1D structure brings in a preferential exposure of low-energy facets, minimizing the surface energy and, consequently, making the NWs more stable than NPs with the same diameter.[14] Meanwhile, 1D motif possesses fewer defects comparing with NPs and thereby a less tendency to be passivated by reactants.[14] Inspired by these recent synthetic advances of the 1D nanocatalysts, we report a unique catalyst based on 1D core–shell-like PtFe–FeO$_x$ NWs supported on TiO$_2$ (denoted as PtFe–FeO$_x$/TiO$_2$) for room temperature CO oxidation. Figure 1A illustrates the synthetic route for PtFe–FeO$_x$/TiO$_2$. The premade PtFe NWs were first assembled onto TiO$_2$ to form the interface between NWs and TiO$_2$. The product was subsequently heated in air to diffuse Fe out onto the surface, forming FeO$_x$ domain. The hierarchical architecture in PtFe–FeO$_x$/TiO$_2$ creates two interfaces including: (1) the atomic interface between the PtFe and metal oxide (FeO$_x$) and (2) the interface between NWs and the support (TiO$_2$). Both interfaces are found to be highly effective in catalyzing CO oxidation through a combination of Mars–van Krevelen (MvK) and Langmuir–Hinshelwood (LH) reaction mechanism.

To prepare PtFe–FeO$_x$/TiO$_2$ nanostructure, PtFe NWs with a width of 4.5 ± 0.3 nm and a length of 20−50 nm were synthesized via a seed-mediated growth, according to a modified previous method (see Supporting Information (SI)).[15,16] The 2.5 ± 0.2 × 20−50 nm PtFe NWs were first synthesized and used as the seeds
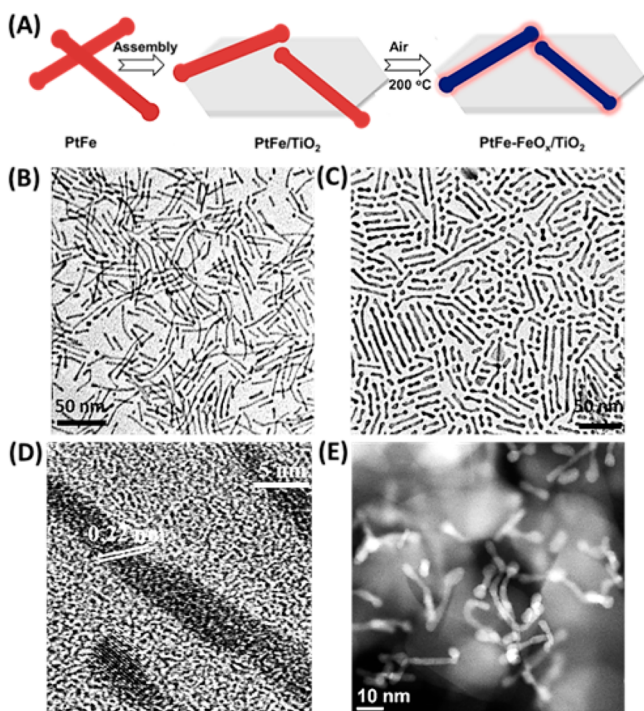
Figure 1. (A) Schematic illustration of the synthesis of TiO_2-supported PtFe−FeO_x NWs. TEM images of the 2.5 × 20−50 nm PtFe NWs (B) and 4.5 × 20−50 nm PtFe NWs (C). (D) HRTEM of the 4.5 × 20−50 nm PtFe NWs. (E) STEM image of the 4.5 × 20−50 nm PtFe−FeO_x NWs supported on TiO_2.

(Figure 1B). To generate the 4.5 ± 0.3 × 20−50 nm PtFe NWs, an equal amount (0.25 mmol) of platinum acetylacetonate ($Pt(acac)_2$) and iron pentacarbonyl ($Fe(CO)_5$) were added into the mixture of oleylamine (OAm), oleic acid (OA), and 1-octadecene (ODE) in the presence of PtFe seeds (SI). For comparison, 4 ± 0.4 nm Pt NPs were synthesized by reducing $Pt(acac)_2$ with borane *tert*-butylamine complex in OAm (SI, Figure S1). Figure 1C shows a representative transmission electron microscopy (TEM) image of the as-synthesized 4.5 ± 0.3 × 20−50 nm PtFe NWs. A typical face centered cubic (*fcc*) structure was observed in the X-ray diffraction (XRD) patterns of both PtFe (width: 2.5 nm) and PtFe (width: 4.5 nm) NWs with their (111) peak positions shifting to a higher angle compared with Pt NPs, indicating the incorporation of Fe into the crystalline lattice (Figure S2A). Furthermore, PtFe (width: 4.5 nm) NWs have an increased domain size and crystallinity, evidenced by the narrower and sharper peaks, than that of PtFe (width: 2.5 nm) NWs (Figure S2A). An interplanar distance of 0.22 nm was obtained from the high-resolution TEM (HRTEM) image, corresponding to the (111) crystalline plane in the *fcc*-PtFe (Figure 1D), similar to the observations in previous reports.[12,17] The Pt to Fe ratio in the seed and final NWs was measured to be ∼1 by inductively coupled plasma optical emission spectroscopy (ICP-OES), indicating a stoichiometric reaction during the synthesis.

The as-synthesized PtFe NWs (width: 4.5 nm) and Pt NPs were deposited on TiO_2 (Degussa P25, surface area 48 m^2/g) through a solution-phase adsorption-assisted assembly (SI). The product, denoted as PtFe/TiO_2, was then annealed in air at 200 °C for 3 h to remove the capping agents and to construct PtFe−FeO_x interfaces. The 1D morphology of the NWs maintained after air annealing, as tracked by scanning electron transmission

microscopy (STEM) (Figure 1E). The 200 °C annealing effectively removed the capping agents, evidenced by the study of *in situ* oxidation of PtFe/TiO_2 NWs on a thermogravimetric analyzer equipped with a mass spectrometer (TGA-MS) (Figure S2B). The steepest weight loss from the TGA and the peak of CO_2 and H_2O production from the MS occurs at 200 °C, corresponding to the thermal decomposition of OAm and OA capped on the NW surface. The removal of the capping agents is further confirmed by Fourier transform infrared (FTIR) spectroscopy, as the strong C−H stretches at 2921 and 2850 cm^{-1} from OAm and OAc disappear after 200 °C annealing (Figure S3). During the annealing, Fe, with a strong O_2 affinity, diffuses out onto the NW surface, forming a thin FeO_x coating, similar to the synthesis of core/shell Au/MnO NPs.[18] The 2D STEM-electron energy loss spectroscopy (EELS) mapping (Figures 2A and S4A) and EELS line scan (Figure S4B) confirm
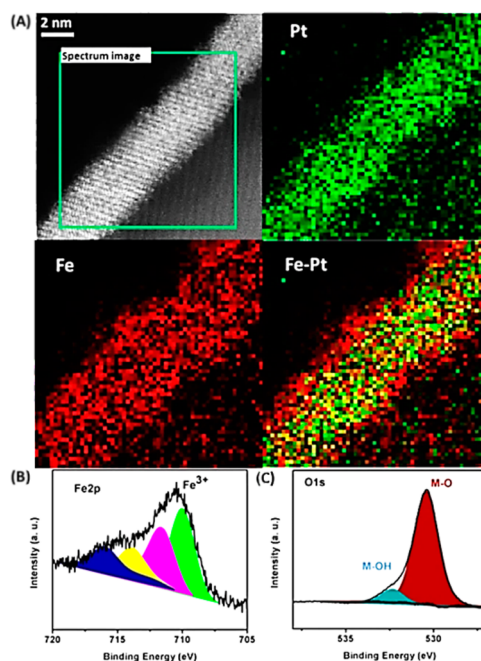

Figure 2. (A) Two-dimensional EELS elemental mapping of Fe (red) and Pt (green). XPS spectra of Fe 2p (B) and O 1s (C).

the enrichment of Fe component on the surface at both the tip and body of the NWs. However, we should notice that the FeO_x on PtFe does not form a compact shell (Figure S4), while a portion of the Pt atoms are exposed. FeO_x formed on PtFe surface is amorphous, characterized by the XRD pattern obtained on the thermally treated PtFe NWs (Figure S5). Further, the X-ray photoelectron spectroscopy (XPS) spectra of Fe 2p show multiplet peaks of Fe^{3+} at 710 eV (Figure 2B). The O 1s spectra suggest a small portion of metal (M)−OH group and a large portion of M−O group, confirming the formation of FeO_x with a Fe valence of 3+ on NW surface (Figure 2C).

The PtFe−FeO_x/TiO_2 and Pt/TiO_2 (ca. 18 mg) were packed into a U-shaped quartz tube (i.d. = 4 mm) and sealed by quartz wool. CO oxidation was then performed with a gas stream consisting of 1% CO (balance air, <4 ppm water) at a space velocity (SV) of 1333 L g^{-1}_{Pt} h^{-1} for PtFe−FeO_x/TiO_2 and 833 L g^{-1}_{Pt} h^{-1} for Pt/TiO_2. The PtFe−FeO_x/TiO_2 readily converted 100% CO starting from room temperature (22 °C), while Pt/TiO_2 displayed negligible CO oxidation activity at temperatures below 88 °C and only achieved 100% conversion starting from

118 °C (Figure 3A). To explore the effect of surface FeO_x, acid leaching was applied to $PtFe-FeO_x/TiO_2$ by immersing the
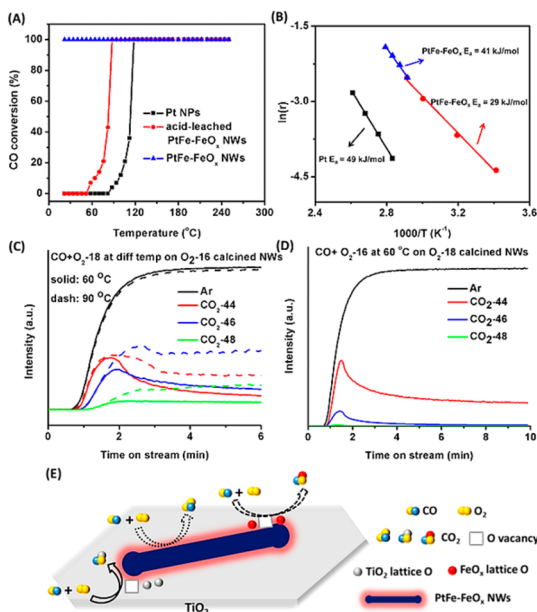

Figure 3. (A) CO oxidation light-off curves for the Pt/TiO_2, $PtFe-FeO_x/TiO_2$, and acid-leached $PtFe-FeO_x/TiO_2$. (B) Activation energies of CO oxidation over $PtFe-FeO_x$ NWs and Pt NPs on TiO_2. QMS profiles collected during CO oxidation with $^{18}O_2$ over $PtFe-Fe^{16}O_x/Ti^{16}O_2$ (C) and with $^{16}O_2$ over $^{18}O_2$ pretreated $PtFe/TiO_2$ (D) at various temperatures. (E) Schematic illustration of two reaction regimes in $PtFe-FeO_x/TiO_2$.

sample in acetic acid (AA) (SI). The removal of surface FeO_x, verified by ~40% Fe loss from ICP, reduced the catalytic activity. Figure 3A shows that the acid-leached NWs start to convert CO at 58 °C and present 100% CO conversion at 88 °C. The CO oxidation activity of acid-leached NWs is higher than that of Pt/TiO_2 because of the Fe incorporation in the core region. This alloy effect is consistent with the reported enhanced CO oxidation on NiPt catalyst.[19] The apparent activation energies (E_a) were derived with a SV of 24000 L g^{-1}_{Pt} h^{-1} on $PtFe-FeO_x/TiO_2$ and 7500 L g^{-1}_{Pt} h^{-1} on Pt/TiO_2. Pt/TiO_2 had an E_a value of 49 kJ mol^{-1}, in agreement with other reports.[11] The E_a was reduced to 41 kJ mol^{-1} (temperature range: 20 to 70 °C) and 29 kJ mol^{-1} (temperature range: 70 to 85 °C) on $PtFe-FeO_x/TiO_2$, proving that incorporation of Fe and FeO_x into Pt facilitates the CO oxidation (Figure 3B). For comparison, $PtFe-FeO_x/SiO_2$, FeO_x/TiO_2, and $PtFe-FeO_x$ NPs/TiO_2 were prepared and tested accordingly (SI).[20] They were all less active than $PtFe-FeO_x/TiO_2$ (Figures S6 and S7). The improved CO oxidation catalysis can be attributed to two synergistic effects of Fe in $PtFe-FeO_x/TiO_2$: (1) The surface FeO_x moiety acts as an active O_2 reservoir to continuously supply O atoms to CO through a redox mechanism and to replenish O from the bulk O_2 lattice.[21] (2) The Fe and FeO_x in the NW modify Pt d-band center to ease the strong CO adsorption on Pt.[9,22−24]

To gain insights into the reaction mechanism on $PtFe-FeO_x/TiO_2$, we performed isotopic labeling experiments by monitoring the exiting stream during the light-off process of CO oxidation via an online quadrupole mass spectrometer (QMS). The $PtFe/TiO_2$ was first treated with $^{16}O_2$ to produce $PtFe-Fe^{16}O_x/TiO_2$ and then reacted with $^{18}O_2$ at both 60 and 90 °C (SI). At the beginning of the reaction, the QMS signal of $^{44}CO_2$ increases

simultaneously with background Ar signal, suggesting only lattice ^{16}O participates in the reaction. As the reaction goes on, the intensity of $^{44}CO_2$ starts to decline, while the signal of $^{46}CO_2$ increases and becomes dominant. Accompanying with the signal of $^{46}CO_2$, $^{48}CO_2$ signal gradually appears (Figure 3C). These results indicate that a mixture of the MvK and LH reaction mechanisms proceeds on $PtFe-FeO_x/TiO_2$ surface at both temperatures. The $^{16}O_2$-treated $PtFe/TiO_2$ reacted with CO and $^{18}O_2$ was further characterized by in situ IR spectroscopy. As shown in Figure S8, two parallel bands at 2356 and 2342 cm^{-1}, associated with $^{44}CO_2$, appear at the beginning of the reaction and decrease in intensity during the reaction. However, the bands at 2342 and 2324 cm^{-1}, which are assigned to $^{46}CO_2$, increase in intensity as the reaction proceeds. This is consistent with the result from QMS that the lattice O reacts first with CO and as the O vacancies are continuously generated, the gas phase O starts to replenish the vacancies and react with CO.

To identify the origination of the lattice O, $PtFe/TiO_2$ was treated with $^{18}O_2$ to form $Fe^{18}O_x$ on the NW surface and then mixed with CO and $^{16}O_2$ at 60 °C (SI). The product was also analyzed by QMS. Along with the signal of Ar and $^{44}CO_2$, $^{46}CO_2$ appears initially and gradually declines, confirming the participation of ^{18}O in FeO_x during CO oxidation (Figure 3D). Figure 3E presents the schematic illustration of the proposed CO oxidation mechanism on the $PtFe-FeO_x/TiO_2$ surface. Two active reaction regimes were observed: (1) The interface between PtFe and FeO_x adopts both MvK mechanism by transferring O atoms from gas phase O_2 to CO through the O vacancy in FeO_x (dash arrow) and LH route by reacting CO directly with adsorbed O_2 from gas phase O_2 (dot arrow). (2) The interface between NWs and TiO_2 follows mainly MvK pathway with lattice O in TiO_2 participating in the reaction (solid arrow). In order to quantify the contribution percentage of each mechanism, the $CO-O_2$ copulse and sequential pulse were performed on $PtFe-FeO_x/TiO_2$ (SI). In the sequential pulse, CO reacts only with lattice O due to the transient exposure to gas phase O_2, providing the information for MvK route. Meanwhile, during the co-pulse, the total CO_2 intensity can be attributed to the sum of MvK and LH routes. As a result, MvK mechanism accounts for over 70% of the generated CO_2, while ~25 to 30% of CO_2 arises from LH route at both 60 and 90 °C (Figure S9). To determine the contribution ratio of lattice O between FeO_x and TiO_2, CO was pulsed onto $^{18}O_2$-treated $PtFe-TiO_2$ and the produced CO_2 was collected. The isotopically labeled CO_2 ($^{46}CO_2$ + $^{48}CO_2$) accounts for 33.3% of the total CO_2 production (Figure S10A). For comparison, Pt/TiO_2 was also treated with $^{18}O_2$ and reacted with CO. In this case, only 6.5% of the total produced CO_2 was isotopically labeled (Figure S10B), confirming the isotopically labeled CO_2 was mainly from $Fe^{18}O_x$. Considering that part of the CO_2 MvK production is from $PtFe-FeO_x$ interface and that LH route contributes significantly at the same time, the $PtFe-FeO_x$ interface serves as a superior active site for CO oxidation.

The effect of Fe, to tune the electronic structure of Pt in PtFe, has been demonstrated by intensive experimental and theoretical studies.[24−27] Hence, the excellent tolerance to CO poisoning can be achieved in Pt−Fe system.[28] To study CO adsorption/desorption behavior, temperature-programmed desorption (TPD) of CO adsorbed on both $PtFe-FeO_x/TiO_2$ and Pt/TiO_2 was tracked by IR spectroscopy (Figure S11). Upon CO adsorption, an intensive band at 2090 cm^{-1}, corresponding to the linear CO−Pt, readily forms on both catalysts. This CO−Pt species is not stable and starts to desorb CO even at room temperature upon switching from CO to inert gas (He) purging

on PtFe−FeO$_x$/TiO$_2$ (Figure S11A). The desorption of CO accelerated with the temperature increase. In comparison with Pt/TiO$_2$ (Figure S11B), PtFe−FeO$_x$/TiO$_2$ adsorbs CO less strongly and CO desorbs at a much lower temperature (Figure S11A). Figure S12 summarizes the CO TPD-MS profile of Pt/TiO$_2$ and PtFe−FeO$_x$/TiO$_2$. A maximum CO desorption was achieved at 54 °C on PtFe−FeO$_x$/TiO$_2$, while on Pt/TiO$_2$ the peak intensity was obtained at 70 °C. This observation proves the incorporation of Fe and FeO$_x$ into Pt alleviates "CO-poisoning" on Pt and promotes CO oxidation. The decay of the room-temperature activity on PtFe−FeO$_x$/TiO$_2$ starts after 40 min on stream (Figure S13A). However, upon purging with O$_2$ for 1 h at slightly heated condition (40 °C), the room-temperature CO conversion arises back to 100% (Figure S13A). This "poisoning" and "recovering" behavior indicates the activity decay is not due to the instability of the catalyst. Instead, it is because that the active sites are blocked by CO at the low temperature and can be reactivated at mild conditions (Figure S13B). For long-term stability study, a time-on-stream test was performed on PtFe−FeO$_x$/TiO$_2$, and the catalyst maintained 100% conversion efficiency after 30 h at 40 °C (Figure S14), consistent with the observation that the strong CO adsorption is eased on PtFe−FeO$_x$/TiO$_2$ at a slightly elevated temperature. The high stability of the catalyst can be attributed to the intact 1D nanostructure during prolonged reaction (Figure S15).

In summary, we have reported a facile synthesis of TiO$_2$-supported PtFe−FeO$_x$ NWs. The interfacial effects on catalysis in PtFe−FeO$_x$/TiO$_2$ have been studied with CO oxidation as a prototype reaction. By taking the advantage of highly active hierarchical interfaces and structural stability of 1D nanostructure, these PtFe−FeO$_x$/TiO$_2$ catalysts demonstrate the superior performance in CO oxidation and achieve 100% CO conversion at room temperature. The strategy of preparing efficient hierarchical interfaces within supported 1D nanostructure provides a unique and promising way to design and fabricate active sites for advanced catalysis.

■ ASSOCIATED CONTENT

Ⓢ Supporting Information

The Supporting Information is available free of charge on the ACS Publications website at DOI: 10.1021/jacs.5b07011.

> Materials, PtFe nanowire, Pt, PtFe, FeO$_x$ nanoparticles synthesis, characterization and their catalytic measurements; Figures S1−S15 (PDF)

■ AUTHOR INFORMATION

Corresponding Authors
*zhuh@ornl.gov
*dais@ornl.gov

Notes
The authors declare no competing financial interest.

■ ACKNOWLEDGMENTS

■ REFERENCES

(1) Wang, Y.; Yoon, Y.; Glezakou, V.; Li, J.; Rousseau, R. *J. Am. Chem. Soc.* **2013**, *135*, 10673.
(2) Widmann, D.; Behm, R. J. *Angew. Chem., Int. Ed.* **2011**, *50*, 10241.
(3) Liu, K.; Wang, A.; Zhang, T. *ACS Catal.* **2012**, *2*, 1165.
(4) Kim, H. Y.; Lee, H. M.; Henkelman, G. *J. Am. Chem. Soc.* **2012**, *134*, 1560.
(5) Liu, H. H.; Wang, Y.; Jia, A.; Wang, S.; Luo, M.; Lu, J. *Appl. Surf. Sci.* **2014**, *314*, 725.
(6) Cargnello, M.; Doan-Nguyen, V. V. T.; Gordon, T. R.; Diaz, R. E.; Stach, E. A.; Gorte, R. J.; Fornasiero, P.; Murray, C. B. *Science* **2013**, *341*, 771.
(7) Wu, Z.; Jiang, D.; Mann, A. K. P.; Mullins, D. R.; Qiao, Z.; Allard, L. F.; Zeng, C.; Jin, R.; Overbury, S. H. *J. Am. Chem. Soc.* **2014**, *136*, 6111.
(8) Peterson, E. J.; DeLaRiva, A. T.; Lin, S.; Johnson, R. S.; Guo, H.; Miller, J. T.; Kwak, J. H.; Peden, C. H. F.; Kiefer, B.; Allard, L. F.; Ribeiro, F. H.; Datye, A. K. *Nat. Commun.* **2014**, *5*, 4885.
(9) Qiao, B.; Wang, A.; Yang, X.; Allard, L. F.; Jiang, Z.; Cui, Y.; Liu, J.; Li, J.; Zhang, T. *Nat. Chem.* **2011**, *3*, 634.
(10) Li, D.; Wang, C.; Strmcnik, D. S.; Tripkovic, D. V.; Sun, X.; Kang, Y.; Chi, M.; Snyder, J. D.; Vliet, D. v. d.; Tsai, Y.; Stamenkovic, V. R.; Sun, S.; Markovic, N. M. *Energy Environ. Sci.* **2014**, *7*, 4061.
(11) Chen, G.; Zhao, Y.; Fu, G.; Duchesne, P. N.; Gu, L.; Zheng, Y.; Weng, X.; Chen, M.; Zhang, P.; Pao, C.; Lee, J.; Zheng, N. *Science* **2014**, *344*, 495.
(12) Zhu, H.; Zhang, S.; Guo, J.; Su, D.; Sun, S. *J. Am. Chem. Soc.* **2013**, *135*, 7130.
(13) Zhu, H.; Zhang, S.; Su, D.; Jiang, G.; Sun, S. *Small* **2015**, *11*, 3545.
(14) Koenigsmann, C.; Santulli, A. C.; Gong, K.; Vukmirovic, M. B.; Zhou, W.; Sutter, E.; Wong, S. S.; Adzic, R. R. *J. Am. Chem. Soc.* **2011**, *133*, 9783.
(15) Guo, S.; Li, D.; Zhu, H.; Zhang, S.; Markovic, N. M.; Stamenkovic, V. R.; Sun, S. *Angew. Chem., Int. Ed.* **2013**, *52*, 3465.
(16) Guo, S.; Zhang, S.; Su, D.; Sun, S. *J. Am. Chem. Soc.* **2013**, *135*, 13879.
(17) Guo, S.; Zhang, S.; Sun, X.; Sun, S. *J. Am. Chem. Soc.* **2011**, *133*, 15354.
(18) Zhu, H.; Sigdel, A.; Zhang, S.; Su, D.; Xi, Z.; Li, Q.; Sun, S. *Angew. Chem., Int. Ed.* **2014**, *53*, 12508.
(19) Mu, R.; Fu, Q.; Xu, H.; Zhang, H.; Huang, Y.; Jiang, Z.; Zhang, S.; Tan, D.; Bao, X. *J. Am. Chem. Soc.* **2011**, *133*, 1978.
(20) (a) Nakaya, M.; Kanehara, M.; Teranishi, T. *Langmuir* **2006**, *22*, 3485. (b) Zhang, S.; Jiang, G.; Filsinger, G. T.; Wu, L.; Zhu, H.; Lee, J.; Wu, Z.; Sun, S. *Nanoscale* **2014**, *6*, 4852.
(21) Li, L.; Wang, A.; Qiao, B.; Lin, J.; Huang, Y.; Wang, X.; Zhang, T. *J. Catal.* **2013**, *299*, 90.
(22) Guo, X.; Fu, Q.; Ning, Y.; Wei, M.; Li, M.; Zhang, S.; Jiang, Z.; Bao, X. *J. Am. Chem. Soc.* **2012**, *134*, 12350.
(23) Fu, Q.; Li, W.; Yao, Y.; Liu, H.; Su, H.; Ma, D.; Gu, X.; Chen, L.; Wang, Z.; Zhang, H.; Wang, B.; Bao, X. *Science* **2010**, *328*, 1141.
(24) Xu, H.; Fu, Q.; Yao, Y.; Bao, X. *Energy Environ. Sci.* **2012**, *5*, 6313.
(25) Zhang, S.; Guo, S.; Zhu, H.; Su, D.; Sun, S. *J. Am. Chem. Soc.* **2012**, *134*, 5060−5063.
(26) Zhang, S.; Zhang, X.; Jiang, G.; Zhu, H.; Guo, S.; Su, D.; Lu, G.; Sun, S. *J. Am. Chem. Soc.* **2014**, *136*, 7734.
(27) Stamenkovic, V. R.; Mun, B. S.; Arenz, M.; Mayrhofer, K. J. J.; Lucas, C. A.; Wang, G.; Ross, P. N.; Markovic, N. M. *Nat. Mater.* **2007**, *6*, 241.
(28) Chen, W.; Kim, J.; Sun, S.; Chen, S. *Langmuir* **2007**, *23*, 11303.